Role of uroguanylin's signalling pathway in the development of ischaemic stroke

Ratko, Martina; Habek, Nikola; Dobrivojević Radmilović, Marina; Škokić, Siniša; Justić, Helena; Barić, Anja; Dugandžić, Aleksandra

Source / Izvornik: **European Journal of Neuroscience, 2022, 56, 3720 - 3737**

Journal article, Published version
Rad u časopisu, Objavljena verzija rada (izdavačev PDF)

https://doi.org/10.1111/ejn.15674

Permanent link / Trajna poveznica: https://urn.nsk.hr/urn:nbn:hr:105:150363

Rights / Prava: Attribution-NonCommercial-NoDerivatives 4.0 International/Imenovanje-Nekomercijalno-Bez prerada 4.0 međunarodna

Download date / Datum preuzimanja: **2024-07-14**

Repository / Repozitorij:

Dr Med - University of Zagreb School of Medicine Digital Repository

Received: 16 November 2021 | Revised: 30 March 2022 | Accepted: 17 April 2022

DOI: 10.1111/ejn.15674

RESEARCH REPORT

EJN European Journal of Neuroscience FENS WILEY

Role of uroguanylin's signalling pathway in the development of ischaemic stroke

Martina Ratko[1,2] | **Nikola Habek**[1,2,3] | **Marina Dobrivojević Radmilović**[1] | **Siniša Škokić**[1] | **Helena Justić**[1] | **Anja Barić**[1] | **Aleksandra Dugandžić**[1,2,3]

[1]Croatian Institute for Brain Research, School of Medicine, University of Zagreb, Zagreb, Croatia

[2]Centre of Excellence for Basic, Clinical and Translational Neuroscience, School of Medicine, University of Zagreb, Zagreb, Croatia

[3]Department of Physiology, School of Medicine, University of Zagreb, Zagreb, Croatia

Correspondence
Aleksandra Dugandžić, Croatian Institute for Brain Research, School of Medicine, University of Zagreb, Šalata 12, Zagreb, Croatia.
Email: aleksandra.dugandzic@mef.hr

Funding information
Croatian Science Foundation, Grant/Award Number: UIP-2017-05-8082; European Regional Development Fund, Grant/Award Number: GA KK01.1.1.01.0007

Edited by: Angeles Almeida

Abstract

Stroke is one of the leading causes of mortality and disability worldwide. By affecting bradykinin function, activation of guanylate cyclase (GC)-A has been shown to have a neuroprotective effect after ischaemic stroke, whereas the same has not been confirmed for GC-B; therefore, we aimed to determine the possible role of GC-C and its agonist, uroguanylin (UGN), in the development of stroke. In this study, middle cerebral artery occlusion (MCAO) was performed on wild-type (WT), GC-C KO and UGN KO mice. MR images were acquired before and 24 h after MCAO. On brain slices 48 h after MCAO, the Ca^{2+} response to UGN stimulation was recorded. Our results showed that the absence of GC-C in GC-C KO mice resulted in the development of smaller ischaemic lesions compared with WT littermates, which is an opposite effect compared with the effects of GC-A agonists on brain lesions. WT and UGN KO animals showed a stronger Ca^{2+} response upon UGN stimulation in astrocytes of the peri-ischaemic cerebral cortex compared with the same cortical region of the unaffected contralateral hemisphere. This stronger activation was not observed in GC-C KO animals, which may be the reason for smaller lesion development in GC-C KO mice. The reason why GC-C might affect Ca^{2+} signalling in peri-ischaemic astrocytes is that GC-C is expressed in these cells after MCAO, whereas under normoxic conditions, it is expressed mainly in cortical neurons. Stronger activation of the Ca^{2+}-dependent signalling pathway could lead to the stronger activation of the Na^{+}/H^{+} exchanger, tissue acidification and neuronal death.

Abbreviations: aCSF, artificial cerebrospinal fluid; AMP, amplifier; ANOVA, analysis of variance; ANP, atrial natriuretic peptide; BL, baseline; bpm, beats per minute; CCA, common carotid artery; cGMP, cyclic guanosine monophosphate; CNG, cyclic nucleotide-gated channel; DAPI, 4′,6-diamidino-2-phenylindole; DEPC, diethyl pyrocarbonate; ECA, external carotid artery; GC-A, guanylate cyclase A; GC-B, guanylate cyclase B; GC-C, guanylate cyclase C; GC-C KO, guanylate cyclase C knock out animals; GFAP, glial fibrillary acidic protein; GUCY2C, gene coding for guanylate cyclase C; HRP, horseradish peroxidase; ICA, internal carotid artery; LDFU, Laser Doppler Flux Unit; MAP, mean arterial pressure; MCA, middle cerebral artery; MCAO, middle cerebral artery occlusion; MR, magnetic resonance; NeuN, neuronal nuclear protein; NHE, sodium proton exchanger; NMDG, *N*-methyl-D-glucamine; PBS, phosphate-buffered saline; ROI, region of interest; SEM, standard error of mean; SR101, sulforhodamine 101; STa, heat-stable enterotoxin; TE, time of echo; TR, time of repetition; UGN, uroguanylin; UGN KO, uroguanylin knockout animals; WT, wild type.

This is an open access article under the terms of the Creative Commons Attribution-NonCommercial-NoDerivs License, which permits use and distribution in any medium, provided the original work is properly cited, the use is non-commercial and no modifications or adaptations are made.
© 2022 The Authors. *European Journal of Neuroscience* published by Federation of European Neuroscience Societies and John Wiley & Sons Ltd.

KEYWORDS
astrocytes, Ca^{2+} signalling, GC-C knockout animals, guanylate cyclase C, UGN knockout animals

1 | INTRODUCTION

Stroke has been recognised as the leading cause of mortality and disability worldwide (Chen et al., 2019), and most cases (75%–80%) are due to ischaemic stroke (Gąsecki et al., 2020). It occurs when a blood clot (either a thrombus or an embolus) causes a significant reduction in blood flow to the brain (Bamford et al., 1991; Hossmann & Schuier, 1980), resulting in irreversible damage to neurons and glia. The ischaemic core, the region most affected by oxygen and nutrient deprivation, undergoes a cascade of events such as disruption in sodium transport, glutamate excitotoxicity, excessive intake of chlorine ions and water, oxidative stress, oedema formation, inflammation and disruption of the blood–brain barrier (Barone & Feuerstein, 1999; Kriz & Lalancette-Hébert, 2009; Lai et al., 2014; Li et al., 2018; Sobey, 2003). The hypoperfused peri-ischaemic region is characterised by the presence of electrophysiologically inactive, but still at least partially metabolically active neurons (González, 2006; Leigh et al., 2018). If blood flow is restored as soon as possible, the viability and function of cells in the peri-ischaemic region can be salvaged; therefore, it has recently become the focus of numerous studies (Gąsecki et al., 2020).

Natriuretic peptides are active in many organs, and their main function is the regulation of blood volume and blood pressure (Pfeifer et al., 1998). Natriuretic peptides, their receptors (membrane guanylate cyclases) and signalling pathways are expressed in the brain (Cao & Yang, 2008; Potter et al., 2006; Sinđić et al., 2011). Mutations in the atrial natriuretic peptide (ANP) or its receptor, guanylate cyclase A (GC-A), have been shown to increase the risk of stroke (Rubattu et al., 1999, 2004). A high plasma ANP concentration is detected in patients up to 1 week after ischaemic stroke (Estrada et al., 1994) and can be used to diagnose ischaemic stroke (Katan et al., 2010). Furthermore, plasma levels of brain natriuretic peptide are in positive correlation to mortality after stroke (Makikallio et al., 2005). Recent studies show that GC-A agonists have neuroprotective effects during stroke development in adult rats (Naruse et al., 1991), whereas guanylate cyclase B (GC-B) agonists have neuroprotective effects during neonatal hypoxic–ischaemic brain injury in mice (Ma & Zhang, 2018). Urodilatin, an ANP isoform, reduces the volume of the ischaemic lesion by inhibiting the effects of bradykinin, which is not observed for the GC-B agonist, C-type natriuretic peptide known as CNP (Dobrivojević et al., 2012, 2016). Listed findings indicate that at least some natriuretic peptides are involved in the pathophysiology of ischaemic stroke and require further research.

To date, guanylate cyclase C (GC-C) is the only known receptor for uroguanylin (UGN). GC-C is found in several brain regions. GC-C is found in the hypothalamic ventral premammillary nucleus (Merlino et al., 2019) and in the arcuate nucleus in humans and laboratory animals (Habek et al., 2020; Kim et al., 2016). GC-C is also located in midbrain dopamine neurons of the ventral tegmental area and substantia nigra (Gong et al., 2011), basolateral amygdaloid nucleus and cortical amygdalar area (Dugandžić et al., 2020). Furthermore, GC-C has been confirmed in mouse cerebral and cerebellar cortex (Habek et al., 2021) and human prefrontal cortex (Colantuoni et al., 2011). In laboratory animals, GC-C is expressed in cortical neurons under physiological conditions, but no expression was found in astrocytes (Habek et al., 2021). UGN, as GC-C agonist, is involved in several brain physiological and pathophysiological functions: satiety regulation (Valentino et al., 2011), browning of white adipose tissue, activation of brown adipose tissue, energy balance (Folgueira et al., 2016; Habek et al., 2021), anxiety (Dugandžić et al., 2020) and attention deficit and hyperactive-like disorder (ADHD) (Gong et al., 2011). However, the potential involvement of UGN in the pathophysiology of ischaemic stroke, as shown for GC-A agonists, is still unknown.

It has been speculated for several decades that UGN may possess another, GC-C-independent, signalling pathway. The existence of a secondary receptor has been recognised for some natriuretic peptides (Fuller et al., 1988). Activation of this 'clearance' receptor (natriuretic peptide receptor C. NPR-C) inhibits adenylate cyclase activity and stimulates the intracellular Ca^{2+} signalling pathway (Anand-Srivastava, 2005). This natriuretic peptide receptor C is downregulated in ischaemic stroke (López-Morales et al., 2018). However, the available evidence confirming the existence of another receptor for UGN is still very scarce. The binding sites for the *Escherichia coli* heat-stable enterotoxin (STa), another GC-C agonist, do not co-localise completely with GC-C in the rat intestine. This secondary binding site showed a higher affinity for STa than GC-C

(Crane et al., 1992), and its activation leads to an increase in intracellular Ca^{2+} concentrations (Ganguly et al., 2001). Studies of kidneys from male GC-C knockout (GC-C KO) animals show that there is no difference in UGN effects when compared with wild-type (WT) animals (Carrithers et al., 2004; Sindić et al., 2005). Taking into account these findings, the existence of a secondary signalling pathway for UGN is expected, though which receptor is involved and its downstream signalling cascade are still mainly unknown (Habek et al., 2021).

Following the study which investigated the role of other natriuretic peptides and their receptors in the pathophysiology of ischaemic stroke, the aim of this study is to determine the role of UGN and its signalling pathways in the development of ischaemic lesion and oedema formation.

2 | MATERIALS AND METHODS

2.1 | Ethics statement

All experimental procedures were approved by the National Ethical Committee (EP 301/2020) and the Ministry of Agriculture (UP/I-322-01/20-01/45). The experiments were conducted in accordance with the Ethical Codex of Croatian Society for Laboratory Animal Science and ARRIVE guidelines. Every effort was made to minimise animal suffering and reduce the number of animals used in the experiments.

2.2 | Animals

All animals used in this study were 6- to 9-month-old (29.69 ± 0.67 weeks) male mice belonging to three separate strains (C57Bl/6NCrl/WT: $n = 7$; GC-C KO: $n = 5$; UGN KO: $n = 6$) and two littermate strains (GC-C littermates: GC-C WT: $n = 14$, GC-C KO: $n = 20$; UGN littermates: UGN WT: $n = 18$, UGN KO: $n = 17$). GC-C KO mice were a donation from Dr K. A. Steinbrecher (Cincinnati Children's Hospital Medical Center, Cincinnati, Ohio, USA). UGN KO mice were a donation from Prof Dr A. P. Naren (Cincinnati Children's Hospital Medical Center, Cincinnati, Ohio, USA) (Begg et al., 2014). The animals were housed in our animal facility (HR-POK-006) and crossbred for generations with our WT strain (C57Bl/6NCrl).

The animals were housed in the same room with controlled environmental conditions (temperature 24 ± 1°C, humidity 53 ± 1%). They were kept on a 12-h light–dark cycle and had access to standard rodent food and water ad libitum.

2.3 | Middle cerebral artery occlusion (MCAO)

Mice were preoperatively injected i.p. with 0.05 mg/kg buprenorphine (Buprenovet, Bayer, Leverkusen, Germany) to ensure adequate analgesia during surgery. Induction of anaesthesia was achieved with 4% isoflurane (Abbott Laboratories Ltd., Kent, UK) in a 30/70 oxygen/air mixture. After ensuring that the animal was adequately anaesthetised, it was placed on a heating pad pre-warmed to 37°C. The isoflurane concentration was reduced to 1.5% and maintained at this level throughout the procedure. Eye gel (Recugel, Bausch & Lomb Inc., Laval, Canada) was applied to both eyes to prevent corneal drying. The surgery was performed under a stereomicroscope (ZEISS Stemi DV4 SPOT Stereomicroscope, Carl Zeiss AG, Oberkochen, Germany) with a cold light source (KL 1500 LCD Light Source, Schott AG, Mainz, Germany).

To measure the changes in blood flow during MCAO, the laser Doppler probe was placed on the temporal bone as follows. After shaving the right temporal region, the skin was disinfected, and an incision was made in the temporal muscle to place the calibrated laser probe (φ 1 mm) above the distal portion of the middle cerebral artery (MCA). Perfusion values were recorded on a laser Doppler perfusion monitor (Moor Instruments, Axminster, UK). Results are presented as Laser Doppler Flux Units (LDFU).

The MCAO surgical procedure was modified according to Belayev et al. (1999). After shaving and disinfection of the surgical field, a midline neck incision was made. The salivary glands and sternocleidomastoid muscle were pulled aside to expose the common (CCA), external (ECA) and internal (ICA) carotid arteries. The CCA was isolated from the surrounding tissue. A 6-0 monofilament thread (Dafilon, B. Braun Surgical SA, Barcelona, Spain) was used to knot the left CCA in two places. The ECA/ICA bifurcation was temporarily clamped with Dumont tweezers No. 7 (Fine Science Tools GmbH, Heidelberg, Germany). A small incision was made in the CCA between the two knots, after which a silicone monofilament (6-0, Doccol Corporation, Sharon, MA, USA) was guided through the incision. After removing the Dumont tweezers, the MCA occlusion was achieved by pushing the monofilament through to the circle of Willis up to the beginning of the MCA and fixing it in place. The wound was closed with temporary clips, and the mouse was moved to a heated cage for 60 min.

After the 60-min occlusion, the mouse was anaesthetised again with isoflurane as described above. The temporary clips were removed along with the

monofilament to allow reperfusion. The neck incision was sutured with 4-0 nylon thread. Postoperatively, the animals were injected with 0.2-ml saline solution to prevent dehydration and 0.25 ml of buprenorphine for analgesia. Softened rodent food and water were freely available in the cages at a lowered height to encourage the animals to eat and prevent excessive weight loss.

MCAO was performed on 40 animals from four experimental groups: GC-C WT, GC-C KO, UGN WT and UGN KO. Fifteen animals were excluded from further experiments (equally distributed among the experimental groups) because they either (a) did not develop an ischaemic stroke due to incomplete MCAO ($n = 3$), (b) developed haemorrhagic stroke most likely due to surgical error ($n = 2$) or (c) died in the 24 h following MCAO ($n = 10$). A successful MCAO surgery, characterised by an ischaemic lesion in cortical, striatal and hippocampal regions, was confirmed in 25 animals with magnetic resonance (MR) imaging.

2.4 | MR imaging

Animals were imaged before MCAO surgery to determine baseline volumes of both hemispheres and 24 h after MCAO to assess the volume of the ischaemic lesion and the size of oedema. MR imaging was performed with a preclinical 7-T Bruker BioSpec 70/20 USR system with Paravision 6.0.1 software (Bruker BioSpin GmbH, Rheinstetten, Germany) in a Tx/Rx configuration using an 86-mm transmit volume coil (MT0381, Bruker BioSpin GmbH) and a two-element mouse brain surface receive coil (MT0042, Bruker BioSpin GmbH) at the GlowLab Laboratory for Regenerative Medicine, School of Medicine, University of Zagreb. Animals were anaesthetised with isoflurane (Abbott Laboratories Ltd.) in a 30/70 O_2/N_2O mixture as described above. Eye moisture was maintained with eye gel (Recugel, Bausch & Lomb Inc.). Body temperature was maintained constant (36.5–37.5°C) using an MR-compatible rectal temperature probe (Medres Medical Research GmbH, Cologne, Germany) and a built-in feedback-controlled circulating heating system. Respiration and cardiac output were monitored throughout the imaging procedure with an optical probe (Medres Medical Research GmbH).

T2-weighted images of the brain were acquired in the coronal plane using a Rapid Acquisition with Relaxation Enhancement sequence with time of echo/time of repetition (TE/TR) = 33/3000 ms; matrix size 166 × 100; field of view 16 × 10 mm^2; slice thickness 0.4 mm; interslice distance 0.1 mm; number of slices 25. T2 maps were obtained using a multi-spin-multi-echo sequence with TE/TR = 8/3500 ms; matrix size 128 × 80; field of view 16 × 10 mm^2; slice thickness 0.4 mm; interslice distance 0.1 mm; number of slices 25. Values were calculated from the measured data using Paravision 6.0.1 software (Bruker BioSpin GmbH) built-in post-processing macros, after which determination of hemisphere and lesion sizes was performed with the ImageJ 1.53i software (Wayne Rasband National Institutes of Health, Bethesda, MD, USA) by two experienced examiners who were blind to the experimental groups. The size of the oedema was presented as the percentage increase in the volume of the ipsilateral hemisphere 24 h after MCAO compared with baseline (BL) volume.

2.5 | Non-invasive blood pressure measurements

All animals were brought to the laboratory the day before the measurements to acclimatise and reduce stress before the procedure. On the day of the experiment, animals were anaesthetised with 4% isoflurane (Abbott Laboratories Ltd.) in a 30/70 O_2/N_2O mixture as described above. After induction of anaesthesia, the animals were placed on a heating pad. Anaesthesia was maintained with 1.4%–1.8% isoflurane and respiration was monitored throughout the procedure. The animals' body temperature was maintained at 37°C–38°C. Eye gel (Recugel, Bausch & Lomb Inc.) was applied to both eyes to prevent corneal drying during anaesthesia.

Blood pressure was measured with the non-invasive tail-cuff method using the CODA® Monitor Noninvasive Blood Pressure System (Kent Scientific Corporation, Torrington, CT, USA). The procedure was performed as suggested by the manufacturer and described previously (Zhao et al., 2011). The following parameters were set in the accompanying software prior to recording: five acclimation cycles followed by one set of 15 cycles with 5 s between cycles. The deflation time was set to 20 s, with a minimum tail blood volume of 15 μL.

Once the desired body temperature and anaesthesia level were achieved, an occlusion cuff was placed at the base of the animal's tail, followed by the volume pressure recording cuff. The recording was started after ensuring proper cuff placement. The following parameters were measured: systolic, diastolic and mean arterial pressure (MAP; mmHg), heart rate (bpm), tail blood volume (μl) and tail blood flow (μl/min).

2.6 | Neurological scoring

To determine neurological impairment after stroke induction, neurological scoring was performed 24 and

48 h after MCAO surgery. Scoring was performed as described previously (Garcia et al., 1995; Li et al., 2000). The following parameters were assessed: loss of body weight, appearance and posture, spontaneous activity, gait disturbances, forelimb placement, body proprioception and reflex testing. The maximum number of points an animal could receive per session was 42. The same researcher performed the scoring assessment and was blind to the animal's experimental group. The scores were divided into five groups (Group 0: 0–10 pts, Group 1: 11–18 pts, Group 2: 19–26 pts, Group 3:27–34 pts, Group 4: 35–42 pts) from which percentages were calculated.

2.7 | Ca^{2+} measurements

Ca^{2+} measurements were performed as previously described (Habek et al., 2021). Briefly, 48 h after MCAO, animals were anaesthetised with i.p. injections of ketamine/xylazine (80–100 and 10–12.5 mg/kg, respectively) and perfused with ice-cold *N*-methyl-D-glucamine (NMDG) artificial cerebrospinal fluid (aCSF) of the following composition: 93 mM NMDG, 93 mM HCl, 2.5 mM KCl, 1.2 mM NaH_2PO_4, 30 mM $NaHCO_3$, 20 mM HEPES (4-(2-hydroxyethyl)piperazine-1-ethanesulfonic acid), 25 mM D-glucose, 10 mM $MgSO_4$, 0.5 mM $CaCl_2$. The brain was isolated, and 250-μm-thick coronal slices were cut using the Leica VT1200S vibrating microtome (Leica Biosystems Nußloch GmbH, Nußloch, Germany). Brain slices underwent short recovery in NMDG aCSF, heated to 33°C. They were then placed in the aCSF solution (127 mM NaCl, 10 mM D-glucose, 1.25 mM NaH_2PO_4, 26 mM $NaHCO_3$, 2 mM $MgSO_4$, 3 mM KCl, 2 mM $CaCl_2$) and left to rest at room temperature for 1 h. The slices were then incubated in a Ca^{2+}-sensitive dye (10 μM, Oregon-Green 488 BAPTA-1, AM, Life Technologies, Carlsbad, CA, USA) and an astrocyte-labelling dye (0.8 μM, sulforhodamine 101 [SR101], Sigma-Aldrich, St. Louis, MO, USA) for 20 min at room temperature under aeration with a 5%CO_2/95%O_2 gas mixture. After rinsing the dyes twice with aCSF for 10 min at room temperature, they were placed in a visualisation chamber and mounted on the Zeiss LSM 510-META confocal microscope (Carl Zeiss AG, Oberkochen, Germany). For the experiment, the cortical regions adjacent to the ischaemic core (peri-ischaemic region) in the ipsilateral and corresponding region of the contralateral hemisphere were located. The Ca^{2+}-sensitive dye was excited with an argon laser line 488, and the emitted signal was collected at 505–530 nm. UGN (PeptaNova GmbH, Sandhausen, Germany) was added to the chamber. Confocal images were taken every second (1 Hz). After the experiment, SR101 was excited by the 543-nm HeNe laser line, and fluorescent signals of both dyes were acquired in one focal plane with a voxel size of 30 μm^3. Regions of interest (ROIs) were selected, and the changes in fluorescence intensities for these ROIs were analysed in MATLAB (MathWorks, Natick, MA, SAD). Of the 260 responding cells, only 12 cells were excluded from further analysis due to non-overlapping BAPTA and SR101 fluorescence, because it could not be determined with certainty whether these were astrocytes. The results are presented as $\Delta F/F_0$ (ratio of the difference in intensity between two consecutive images and the background signal).

2.8 | Immunohistochemistry

Two different approaches were used to determine the localisation of GC-C: immunohistochemistry and in situ hybridisation. After Ca^{2+} measurements, 48 h after MCAO, the residual brain slices were used for immunohistochemistry. The slices were fixed in 4% paraformaldehyde (Biognost Ltd., Zagreb, Croatia) overnight at 4°C. After fixation, they were cryoprotected in the following manner: incubation in a 0.01 M phosphate-buffered saline (PBS) solution (pH 7.4) with rising sucrose concentrations (10%, 20%, 30%), after which they were transferred to a cryoprotectant solution (0.01 M PBS, 30% sucrose, 1% polyvinylpyrrolidone, 30% ethylene-glycol) and frozen at −20°C.

On the day of the experiment, brain slices were thoroughly rinsed with 0.01 M PBS for 90 min. Antigen retrieval was performed by boiling the slices in 0.01 M citrate buffer (pH 6.0) for 20 min. After allowing the slices to cool to room temperature, they were rinsed with 0.01 M PBS three times for 10 min at room temperature. Permeabilisation was achieved by incubating the samples in 0.4% Tween 20 in 0.01 M PBS for 15 min. After rinsing the detergent as written above, brain slices were incubated in a blocking buffer (1% bovine serum albumin [Sigma-Aldrich] in 0.01 M PBS) for 1 h at room temperature. The brain slices were incubated with rabbit polyclonal anti-GC-C antibody (1:50; OACA09780, Aviva Systems Biology, San Diego, CA, USA) overnight at 4°C. Slides were rinsed three times for 10 min with 0.01 M PBS at room temperature before incubation with the secondary donkey polyclonal anti-rabbit antibody (1:500; A32795, Alexa Fluor Plus 647, Invitrogen, Carlsbad, CA, USA) for 1 h at room temperature. After rinsing as described above, brain slices were then incubated with mouse monoclonal anti-NeuN (neuronal nuclear protein) antibody (1:500; MAB377, Sigma-Aldrich) overnight, followed by rinsing steps described above, and incubation with the secondary donkey polyclonal anti-mouse

antibody (A32766, Alexa Fluor Plus 488, Invitrogen) for 1 h at room temperature. Mowiol mounting solution (Merck KGaA, Darmstadt, Germany) was applied, and the slices were covered with coverslips.

Prepared brain slices were mounted on the FV3000 confocal laser scanning microscope (Olympus Corp., Shinjuku, Tokyo, Japan). Peri-ischaemic ipsilateral cortex and their corresponding regions in the contralateral hemisphere were located. Fluorescent signals were induced with the 488- and 640-nm laser lines, and fluorescent signal was collected at 500–540 and 650–750 nm for NeuN and GC-C, respectively, at one focal plane and voxel size of 0.09 μm^3.

2.9 | In situ hybridisation by RNAScope

The GC-C mRNA localisation in the ipsilateral and contralateral hemispheres after MCAO was determined by RNAScope® assay (GC-C assay, Mm-Gucy2C, 436591, Advanced Cell Diagnostics, Newark, CA). Forty-eight hours after MCAO, the WT animal was anaesthetised with ketamine/xylazine (80–100 and 10–12.5 mg/kg, respectively) and perfused first with 0.01 M PBS solution (pH 7.4) and later with 4% paraformaldehyde (Biognost Ltd.). The entire brain was isolated and fixed in 4% paraformaldehyde (Biognost Ltd.) overnight at 4°C and cryoprotected as described above. 60-μm brain slices were cut using the Leica CM1950 cryostat (Leica Biosystems Nußloch GmbH) and mounted on positively charged Superfrost Plus slides (Thermo Fisher Scientific, Waltham, MA, USA).

Following procedures were performed as suggested by the manufacturer (RNAScope Multiplex Fluorescent Detection Reagents v2, product code:323110, Advanced Cell Diagnostics) (Ikpa et al., 2016; Wang et al., 2012). Briefly, brain slices were washed three times per 10 min with 0.01 M PBS-DEPC (diethyl pyrocarbonate) solution (Sigma-Aldrich) and incubated in 3% hydrogen peroxide (product code: 322381) for 10 min at room temperature. After rinsing three times per 10 min in 0.01 M PBS-DEPC, the slices underwent target retrieval (product code 322001) for 15 min at 95°C, washed three times in 0.01 M PBS-DEPC after which they were incubated in Protease IV (product code: 322381) for 30 min at 40°C. Slices were rinsed with 0.01 M PBS-DEPC as described above and incubated in a humidity control chamber with a GC-C probe for 2 h at 40°C. Signal amplification was achieved by sequential incubation in amplifier (AMP) 1, AMP 2 and AMP 3 reagent at 40°C for 30, 30 and 15 min, respectively. Between incubations, the samples were thoroughly rinsed with a wash buffer (product code: 310091). Signal detection was performed by incubating the slices in HRP (horseradish peroxidase)-C1 activator for 15 min at 40°C. After a short wash in wash buffer, TSA fluorescein dye (1:100, excitation: 494 nm, emission: 517 nm, Akoya Biosciences, Marlborough, MA, USA) was added, and the sample was incubated for 30 min at 40°C. After a short wash in wash buffer, the sample was incubated in HRP Blocker for 15 min at 40°C. Amplified mRNA for GC-C will be presented as dots.

After in situ hybridisation, slices were thoroughly rinsed three times for 10 min with 0.01 M PBS and 0.1% Triton X-100 (Sigma-Aldrich) at room temperature. Slices were rinsed three times for 10 min with 0.01 M PBS and 0.1% Triton X-100 and incubated in blocking solution (0.01 M PBS, 0.1% Triton X-100, 1% bovine serum albumin) for 2 h at room temperature. Chicken polyclonal antibody (ab134436, Abcam, Cambridge, UK) for glial fibrillary acidic protein (GFAP) was used to label astrocytes. Slices were incubated in the primary antibody (1:100) at 4°C overnight. After rinsing three times for 10 min with 0.01 M PBS at room temperature, they were incubated in goat polyclonal anti-chicken Alexa Fluor® 555 antibody (1:500, ab150170, Abcam) for 1 h at room temperature. Lastly, the slices were incubated in a DAPI (4′,6-diamidino-2-phenylindole) solution (1:4000; Thermo Fisher Scientific) for 5 min at room temperature. After rinsing the dye three times for 10 min in 0.01 PBS, ProLong™ Diamond Antifade Mountant mounting solution (Invitrogen™, Thermo Fisher Scientific) was applied, and the slices were covered with a coverslip.

Stained slices were mounted on the FV3000 confocal laser scanning microscope (Olympus Corp.). GC-C mRNA fluorescent signal was induced with the 488-nm laser line, whereas the signals for DAPI and GFAP were induced with the 405- and 561-nm laser lines, respectively, at seven focal planes and voxel size of 0.07 μm^3. Emitted signals were collected at 430–470, 500–540 and 570–670 nm for DAPI, GC-C, and GFAP fluorescent signals, respectively.

2.10 | Statistical analysis

Data are presented as mean ± SEM unless stated otherwise. For Ca^{2+} experiments, the animal groups consisted of a minimum of three animals. Normality of distribution was tested with the Kolmogorov–Smirnov test. Student's *t*-test was used to compare two variables, and ANOVA with a post hoc Tukey test was used if more than two parameters were analysed, $p < .05$ was considered significant for both analyses. The correlations were assessed with the Pearson correlation test.

Data for neurological impairment assessment were analysed with two non-parametric tests: The

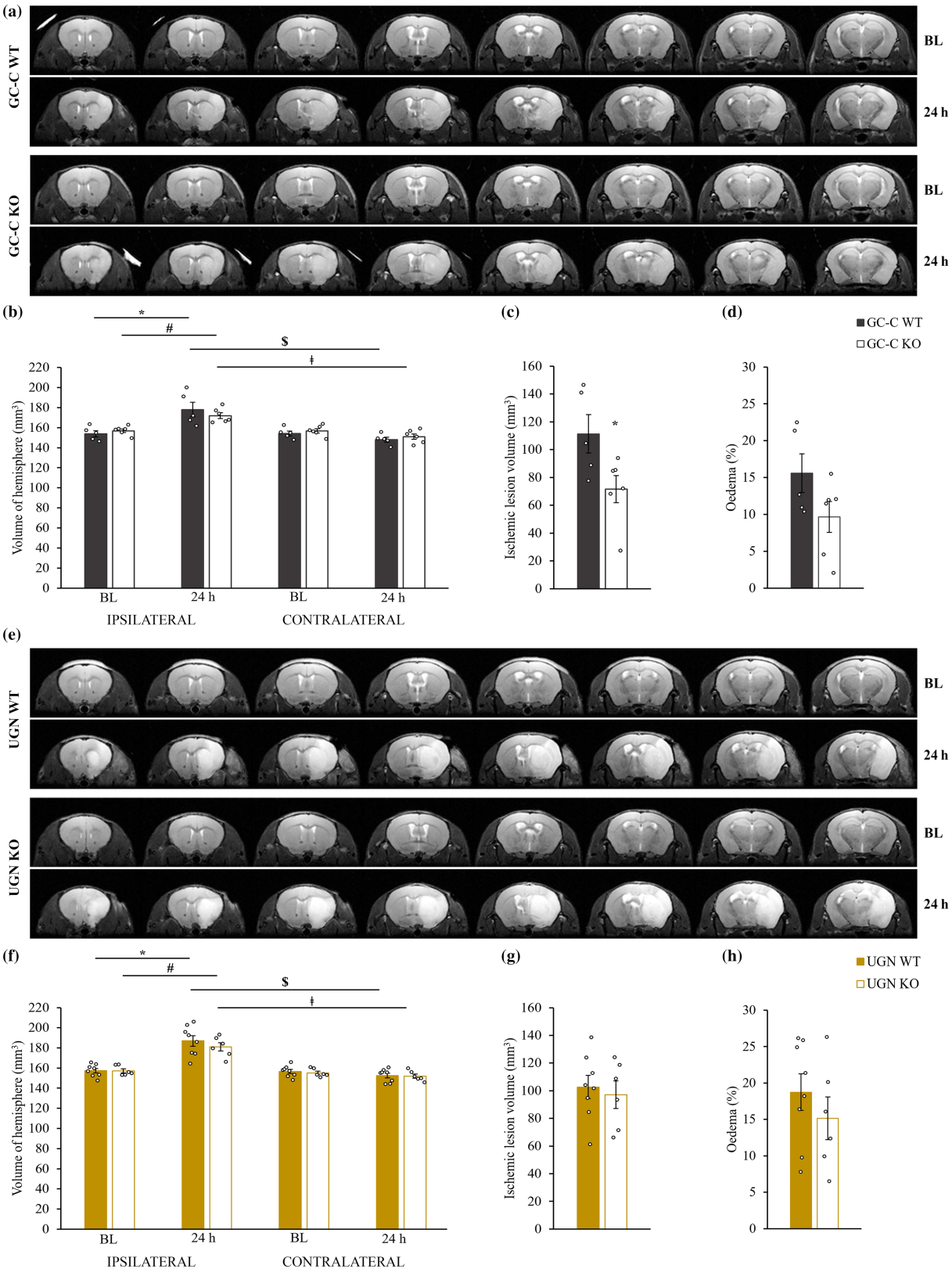

FIGURE 1 Legend on next page.

FIGURE 1 Smaller ischaemic lesion in GC-C KO mice. Volumetric analysis of hemispheres, lesion volumes and oedema size in GC-C WT ($n = 5$), GC-C KO ($n = 6$), UGN WT ($n = 8$) and UGN KO ($n = 6$) animals was performed by MR imaging. (a) The original MR images of ischaemic lesions of GC-C WT and GC-C KO animals taken before (BL) and after MCAO (24 h) are shown. (b) In GC-C KO animals and their WT littermates (GC-C WT), there was a statistically significant increase in the volume of the ipsilateral hemisphere 24 h after MCAO. At the same time point, the volume of the ipsilateral hemisphere was bigger than the contralateral hemisphere in both groups of animals. Data were analysed with an unpaired ANOVA test with a post hoc Tukey test. *$p = .0004$ statistically significant difference between ipsilateral hemispheres of GC-C WT mice before and after MCAO; #$p = .0355$ statistically significant difference between ipsilateral hemispheres of GC-C KO mice before and after MCAO; \$$p = .00001$ statistically significant difference between ipsilateral and contralateral hemispheres of GC-C WT mice 24 h after MCAO; ǂ$p = .001$ statistically significant difference between ipsilateral and contralateral hemispheres of GC-C KO mice 24 h after MCAO ($F(7,36) = 9.727$, $p = 1 \times 10^{-8}$). (c) GC-C KO animals developed significantly smaller ischaemic lesions when compared with GC-C WT animals. *$p = .0386$. (d) No difference in oedema size was observed between the two test groups. Data were analysed with unpaired Students *t*-test. (e) The original MR images of ischaemic lesions of UGN WT and UGN KO animals taken before (BL) and after MCAO (24 h) are shown. (f) In UGN KO animals and their WT littermates (UGN WT), there was an increase in the volume of the ipsilateral hemisphere 24 h after MCAO. At the same time point, the volume of the ipsilateral hemisphere was bigger than the contralateral hemisphere in both groups of animals. Data were analysed with an unpaired ANOVA test with a post hoc Tukey test. *$p = 6 \times 10^{-8}$ statistically significant difference between ipsilateral hemispheres of UGN WT mice before and after MCAO; #$p = .0001$ statistically significant difference between ipsilateral hemispheres of UGN KO mice before and after MCAO; \$$p = 9 \times 10^{-10}$ statistically significant difference between ipsilateral and contralateral hemispheres of UGN WT mice 24 h after MCAO; ǂ$p = .000003$ statistically significant difference between ipsilateral and contralateral hemispheres of UGN KO mice 24 h after MCAO ($F(7,48) = 20.490$, $p = 2 \times 10^{-12}$). (g) UGN littermates developed similar lesion sizes. (h) No difference in oedema size was observed between the two test groups. Data were analysed with unpaired Students *t*-test. Data are presented as mean ± SEM. BL, baseline (volume of the hemispheres before MCAO)

TABLE 1 Ischaemic lesion volume (mm^3) of male mice 24 h after MCAO

GC-C WT ($n = 5$)	GC-C KO ($n = 6$)	UGN WT ($n = 8$)	UGN KO ($n = 6$)
111.30 ± 13.80	71.55 ± 9.70*	102.68 ± 8.41	97.05 ± 9.95

*Statistically significant difference when compared with GC-C WT mice ($p = .0386$).

Kruskal–Wallis test was used for intergroup comparisons, and paired Wilcoxon test was used to verify whether animals developed more severe neurological symptoms 48 h compared with 24 h after MCAO. Statistical analysis was performed with the GraphPad Instat (GraphPad Software, San Diego, CA, USA).

3 | RESULTS

3.1 | Smaller ischaemic lesions in GC-C KO animals

To investigate whether UGN has an impact on ischaemic lesion size, 60-min MCAO was performed. The original MR images are shown in Figure 1a,e. Baseline (BL) measurements of both ipsilateral and contralateral hemisphere volumes did not differ between test groups (Figure 1b,f).

A significant increase in ipsilateral hemisphere volume 24 h after MCAO compared with BL volumes was shown for both GC-C WT and KO animals ($F(3,18) = 8.134$, $p = .001$) as well as UGN littermates ($F(3,24) = 17.473$, $p = .000003$). Contralateral hemispheres did not change in volume after stroke induction in all tested animals. Contralateral hemispheres were significantly smaller when compared with ipsilateral ones 24 h after MCAO.

An interesting finding was that GC-C KO animals had 35% smaller ischaemic lesions compared with GC-C WT animals ($p = .0386$; Figure 1c, Table 1), whereas UGN littermates showed no difference between groups ($p = .6716$; Figure 1g, Table 1). However, the enlargement of the ipsilateral brain hemisphere due to ischaemic lesion and brain oedema formation (Figure 1d,h) did not significantly differ between GC-C ($p = .106$) or UGN littermates ($p = .372$).

The possible reason for the difference in size of the brain lesion is the difference in blood pressure or a difference in the reduction of the blood flow during MCAO. Because it was shown that UGN KO animals have higher blood pressure compared with WT littermates (Lorenz et al., 2003), we determined the blood pressure in GC-C and UGN littermates as well as in WT, GC-C and UGN KO separate strains. When comparing the individual WT ($n = 6$), GC-C KO ($n = 5$) and

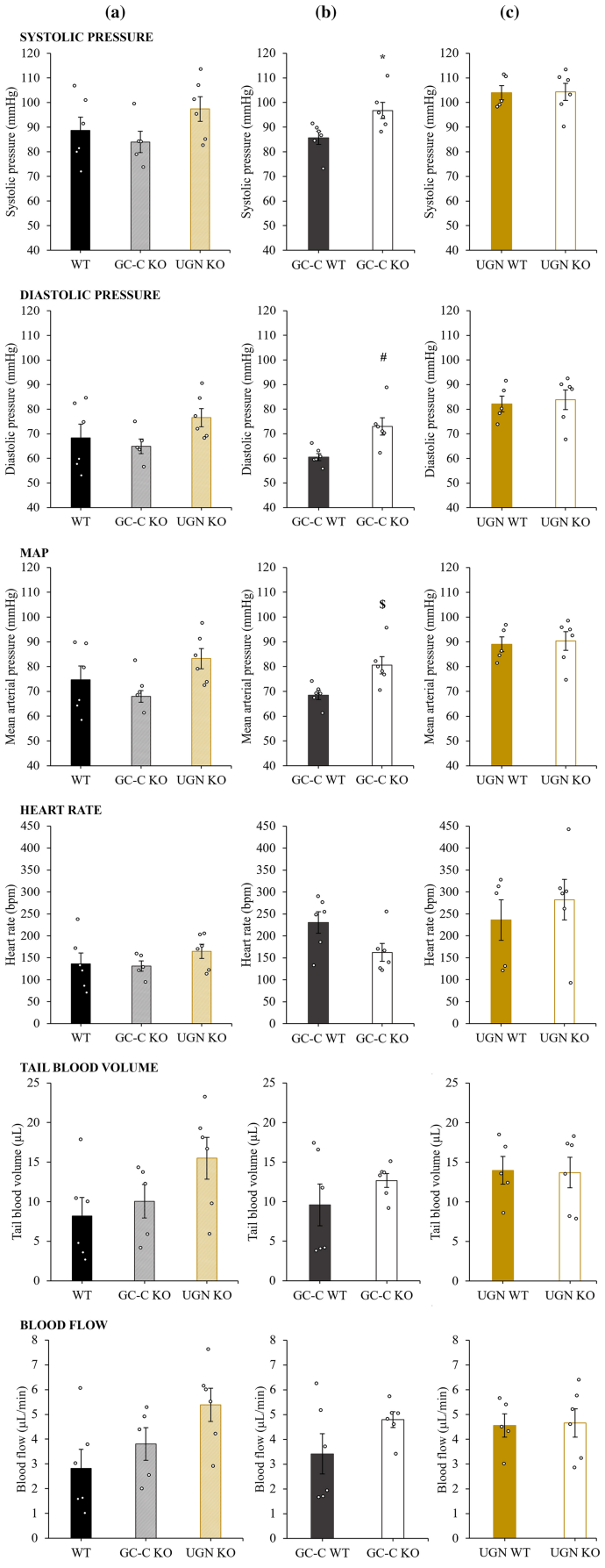

FIGURE 2 Legend on next page.

FIGURE 2 Higher blood pressure in GC-C KO mice when compared with their WT littermates. Systolic pressure, diastolic pressure, mean arterial pressure (MAP), heart rate, tail blood volume and blood flow were measured for separate strains (a; WT: $n = 6$; GC-C KO: $n = 5$; UGN KO: $n = 6$), GC-C littermates (b; GC-C WT: $n = 6$; GC-C KO: $n = 6$) and UGN littermates (c; UGN WT: $n = 5$; UGN KO: $n = 6$). GC-C KO animals had higher systolic, diastolic and MAP than their WT (GC-C WT) littermates, although no difference was found in UGN littermates. Data were analysed with unpaired ANOVA test with post hoc Tukey test (a) or unpaired students *t*-test (b and c). *$p = .026$ statistically significant difference of systolic blood pressure between GC-C KO and GC-C WT littermates. #$p = .009$ statistically significant difference of diastolic blood pressure between GC-C KO and GC-C WT littermates. $$p = .011$ statistically significant difference of MAP between GC-C KO and GC-C WT littermates. Data are presented as mean ± SEM. bpm, beats per minute

UGN KO ($n = 6$) strains, there was no difference between systolic pressure ($F(2,14) = 1,802$, $p = .201$), diastolic pressure ($F(2,14) = 1,863$, $p = .192$), MAP ($F(2,14) = 1,900$, $p = .186$), heart rate ($F(2,14) = ,887$, $p = .434$), tail blood volume ($F(2,14) = 2,574$, $p = .112$), nor blood flow ($F(2,14) = 3,498$, $p = .059$) (Figure 2a). However, when the measured results were compared between WT and KO littermates, different results were obtained. Statistically higher blood pressures were observed in GC-C KO animals ($n = 6$) compared with their WT ($n = 6$) littermates (Figure 2b; systolic pressure: $p = .026$; diastolic pressure: $p = .009$; MAP: $p = .011$) with no difference in heart rate ($p = .058$), tail blood volume ($p = .296$) nor tail blood flow ($p = .142$). However, we did not observe difference in the measured values in UGN KO ($n = 6$) when compared with their WT ($n = 5$) littermates (Figure 2c; systolic pressure: $p = .947$; diastolic pressure: $p = .745$; MAP: $p = .795$; heart rate: $p = .500$; tail blood volume: $p = .918$; tail blood flow: $p = .899$).

Even though there was a difference in blood pressures between GC-C KO and WT littermates, blood flow during MCAO (GC-C WT: 70.0 ± 5.2 LDFU, $n = 5$; GC-C KO: 70.0 ± 3.7 LDFU, $n = 6$, $p = .999$) and its reduction (GC-C WT: 22.5 ± 1.3%, n = 5; GC-C KO: 21.0 ± 1.4%, $n = 6$, $p = .433$) did not differ between groups. In addition, the size of the ischaemic lesion and brain oedema in all tested animals (Figure 3) did not correlate with the remaining blood flow during MCAO (lesion size: $r = .408$, $p = .093$, $n = 18$; brain oedema: $r = .431$, $p = .074$, $n = 18$), suggesting the effects of animal strain on lesion size.

Development and severity of neurological symptoms after ischaemic brain injury were tested on all animals 24 and 48 h after MCAO surgery. Points awarded for each noted neurological deficit were added for each animal and time point. Scores were divided into five groups by severity of the symptoms (Group 0: 0–10 pts, Group 1: 11–18 pts, Group 2: 19–26 pts, Group 3:27–34 pts, Group 4: 35–42 pts), and percentages of tested animals belong to each group were calculated (Figure 4).

Twenty-four hours after MCAO, there was positive correlation between size of the brain lesion and detected

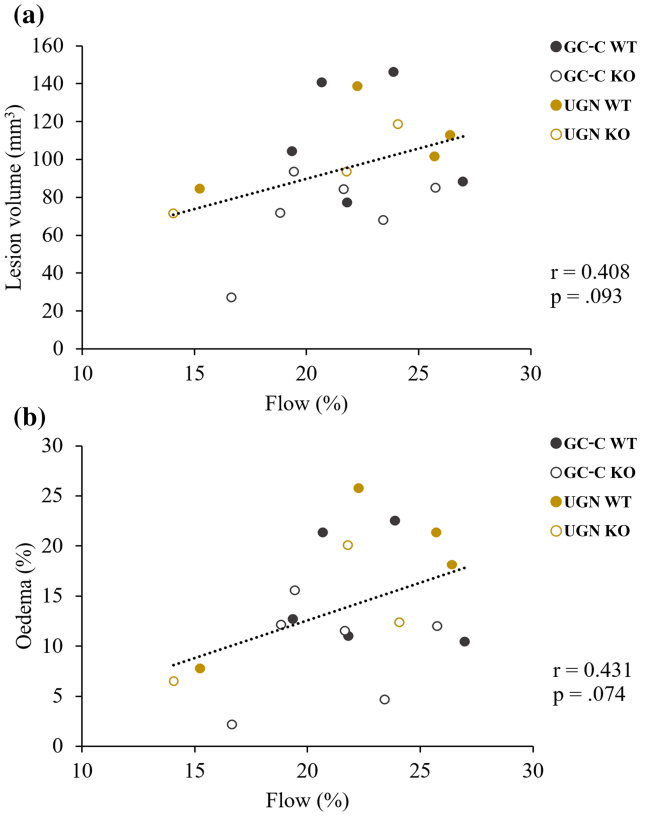

FIGURE 3 No correlation between blood flow during MCAO and lesion size or oedema formation. Neither lesion volume (a; $r = .408$, $p = .093$, $n = 18$) nor oedema size (b; $r = .431$, $p = .074$, $n = 18$) showed significant correlations with blood flow reduction. Data were analysed with Pearson correlation test

neurological symptoms (Figure 4c; $r = .480$, $p = .015$, $n = 25$), whereas while brain oedema did not correlate significantly with symptoms ($r = .382$, $p = .060$, $n = 25$). There was no change in the severity of the symptoms 48 h after MCAO (Figure 4b; GC-C WT: $p = .250$, $n = 3$; GC-C KO: $p = .063$, $n = 5$; UGN WT: $p = .125$, $n = 4$; UGN KO: $p = .063$, $n = 5$). At that time point, there was positive correlation between size of the brain lesion and detected neurological symptoms (Figure 4d; $r = .675$, $p = .003$, $n = 17$), whereas again the brain oedema was not in correlation with symptoms ($r = .347$, p = .172, $n = 17$). There was no statistically significant difference

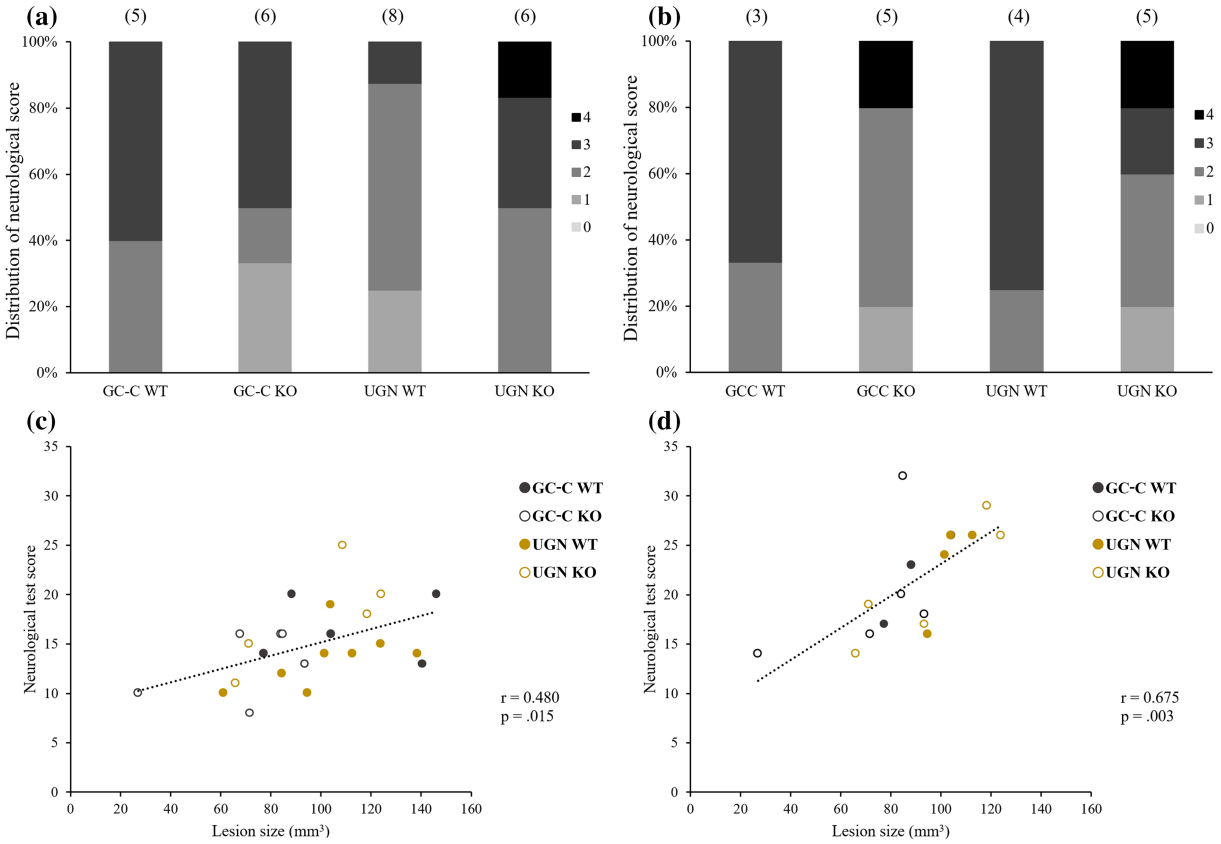

FIGURE 4 No difference in the severity of the symptoms 24 (a) and 48 h (b) after MCAO. Points awarded for each noted neurological deficit were added for each animal. Individual scores were divided into five groups, and percentages of tested animals belonging to each group are shown. The severity of the symptoms was analysed with the Kruskal–Wallis test. Number of animals is shown in brackets. Lesion size showed a positive correlation with neurological scores both 24 (c) and 48 h (d) after MCAO. Data were analysed with the Pearson correlation test

between all tested groups of animals in severity of neurological symptoms at both time points.

3.2 | Stronger Ca^{2+} response in peri-ischaemic astrocytes of UGN KO and WT animals

To determine the effects of UGN on the Ca^{2+} signalling pathway in astrocytes, 48 h after MCAO, brain slices of at least three animals per group were incubated with Oregon-Green 488 BAPTA-1, AM (10 μM) and SR101 (0.8 μM, astrocyte marker).

As shown in Figure 5a, peri-ischaemic astrocytes of the ipsilateral hemispheres of WT animals had a statistically significant increase in Ca^{2+} response to UGN (100 nM) when compared with the same cortical region of the contralateral hemisphere (ipsilateral hemisphere: 7.47 ± 0.46, $n = 53$; contralateral hemisphere: 5.68 ± 0.34, $n = 68$, $p = .002$). This difference was not present in GC-C KO animals (Figure 5b; ipsilateral hemisphere: 5.42 ± 0.39, $n = 30$; contralateral hemisphere: 5.93 ± 0.52, $n = 38$, $p = .459$). However, UGN KO animals, like WT, also showed a difference in the Ca^{2+} response between hemispheres (ipsilateral hemisphere: 9.41 ± 1.1, $n = 37$; contralateral hemisphere: 5.78 ± 0.59, $n = 22$, $p = .018$). The response in both hemispheres of WT animals lasted for a second. The Ca^{2+} response in GC-C KO and UGN KO lasted longer as follows: In the contralateral hemispheres, the response lasted for 2 and 7 s, respectively. In ipsilateral hemispheres, the response was even longer and lasted 3 s in GC-C KO animals and 17 s in UGN KO (the response was determined by statistically significant difference to the value of 1) (Figure 5c).

When the Ca^{2+} response in ipsilateral and contralateral hemispheres of different groups of animals was compared, the response was not different in the contralateral hemispheres of KO animals compared with their WT littermates (Figure 5d,f). However, the Ca^{2+} response in ipsilateral hemispheres was different in UGN KO and GC-C KO. In the ipsilateral peri-ischaemic region, the

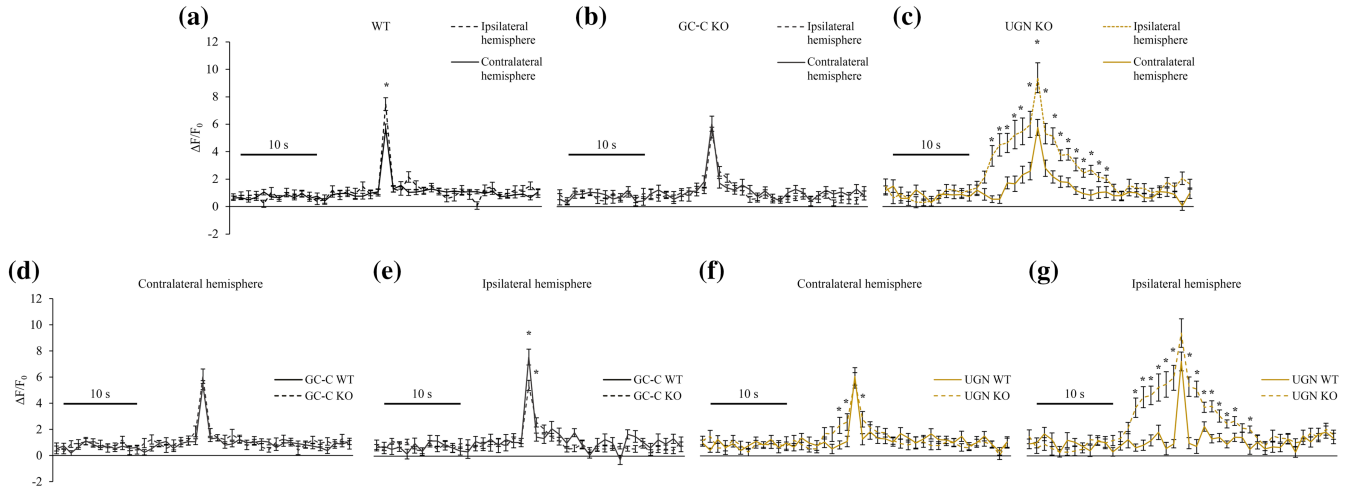

FIGURE 5 Smaller Ca^{2+} response in peri-ischaemic astrocytes of GC-C KO animals. Changes in intracellular Ca^{2+} concentration in astrocytes after UGN stimulation (100 nM) is shown as $\Delta F/F_0$. (a) Summarised results for both wild-type (WT) littermate groups (GC-C WT and UGN WT) showed a significant increase in Ca^{2+} signalling in the ipsilateral hemisphere compared with the contralateral hemisphere (*$p = .002$). (b) GC-C KO animals showed no difference in Ca^{2+} signalling after UGN stimulation between hemispheres. (c) UGN KO animals exhibited an increased Ca^{2+} response for 17 s in the ipsilateral hemisphere when compared with the contralateral hemisphere (*$p = .0005–.0387$). (d) No difference in Ca^{2+} signal was recorded in the contralateral hemisphere of GC-C WT ($n_{animals} = 4$, $n_{slices} = 8$, $n_{cells} = 40$) and GC-C KO animals ($n_{animals} = 3$, $n_{slices} = 6$, $n_{cells} = 38$). (e) GC-C KO animals ($n_{animals} = 3$, $n_{slices} = 6$, $n_{cells} = 30$) showed a significant smaller Ca^{2+} response to UGN stimulation compared with GC-C WT ($n_{animals} = 4$, $n_{slices} = 7$, $n_{cells} = 34$) animals in the ipsilateral hemisphere affected by stroke (*p = .005–.018). (f) No difference in strength of Ca^{2+} response was recorded in the contralateral hemisphere of UGN WT ($n_{animals} = 3$, $n_{slices} = 5$, $n_{cells} = 28$) and UGN KO ($n_{animals} = 3$, $n_{slices} = 6$, $n_{cells} = 22$) animals, but the Ca^{2+} response in UGN KO animals was prolonged for 3 s (*$p = .025–.047$ statistically significant difference between UGN WT and UGN KO Ca^{2+} responses). (g) Ca^{2+} response to UGN stimulation in UGN KO animals ($n_{animals} = 3$, $n_{slices} = 6$, $n_{cells} = 37$) was of similar intensity to UGN WT animals ($n_{animals} = 3$, $n_{slices} = 5$, $n_{cells} = 19$), but was significantly longer (*$p = .00002–.02789$ statistically significant difference between UGN WT and UGN KO Ca^{2+} responses). Data were analysed by unpaired Students *t*-test. Data are presented as mean ± SEM. The bar indicates a length of 10 s

Ca^{2+} signal appeared significantly reduced when compared with their WT littermates (Figure 5e; GC-C WT: 7.59 ± 0.6, $n = 34$; GC-C KO: 5.42 ± 0.39, $n = 30$, $p = .005$). GC-C KO animals showed the same response in both affected (ipsilateral) and contralateral hemispheres (Figure 5b). However, in the peri-ischaemic area of the ipsilateral hemispheres, the intensity of astrocytes' Ca^{2+} signal in UGN KO animals was similar to the affected hemispheres of UGN WT animals (Figure 5g; UGN WT: 7.25 ± 0.73, $n = 19$; UGN KO: 9.41 ± 1.1, $n = 37$, $p = .188$).

3.3 | GC-C expression in peri-ischaemic astrocytes

48 hours after MCAO surgery, brain slices of WT, GC-C KO and UGN KO animals were stained with anti-GC-C antibody and NeuN antibody, a neuronal marker (Figure 6). In the contralateral cortex, both WT (GC-C WT is shown) and UGN KO animals showed co-localisation of NeuN and GC-C, indicating that the GC-C receptor is expressed in cortical neurons as shown in our previous publication (Habek et al., 2021). GC-C KO animals were used as negative control and show no GC-C expression.

The difference in Ca^{2+} response was determined in astrocytes of the peri-ischaemic area in GC-C KO animals compared with WT littermates. Because in physiological conditions astrocytes do not express GC-C, the question was how then GC-C affect the Ca^{2+} signalling in those cells (Habek et al., 2021). A relevant finding was noted in the peri-ischaemic area of the ipsilateral cortex of WT and UGN KO animals. In this region, the pattern of GC-C expression was changed, GC-C rarely co-localised with NeuN, indicating that after ischaemic stroke, GC-C was expressed in another cell type.

To confirm the difference in GC-C expression in astrocytes in physiological versus ischaemic conditions now at mRNA level, in situ hybridisation with a GC-C probe followed by anti-GFAP staining was performed on ipsilateral and contralateral hemispheres of WT animals 48 h after MCAO (Figure 7). GC-C mRNA was present in the peri-ischaemic cortical astrocytes (GFAP-expressing

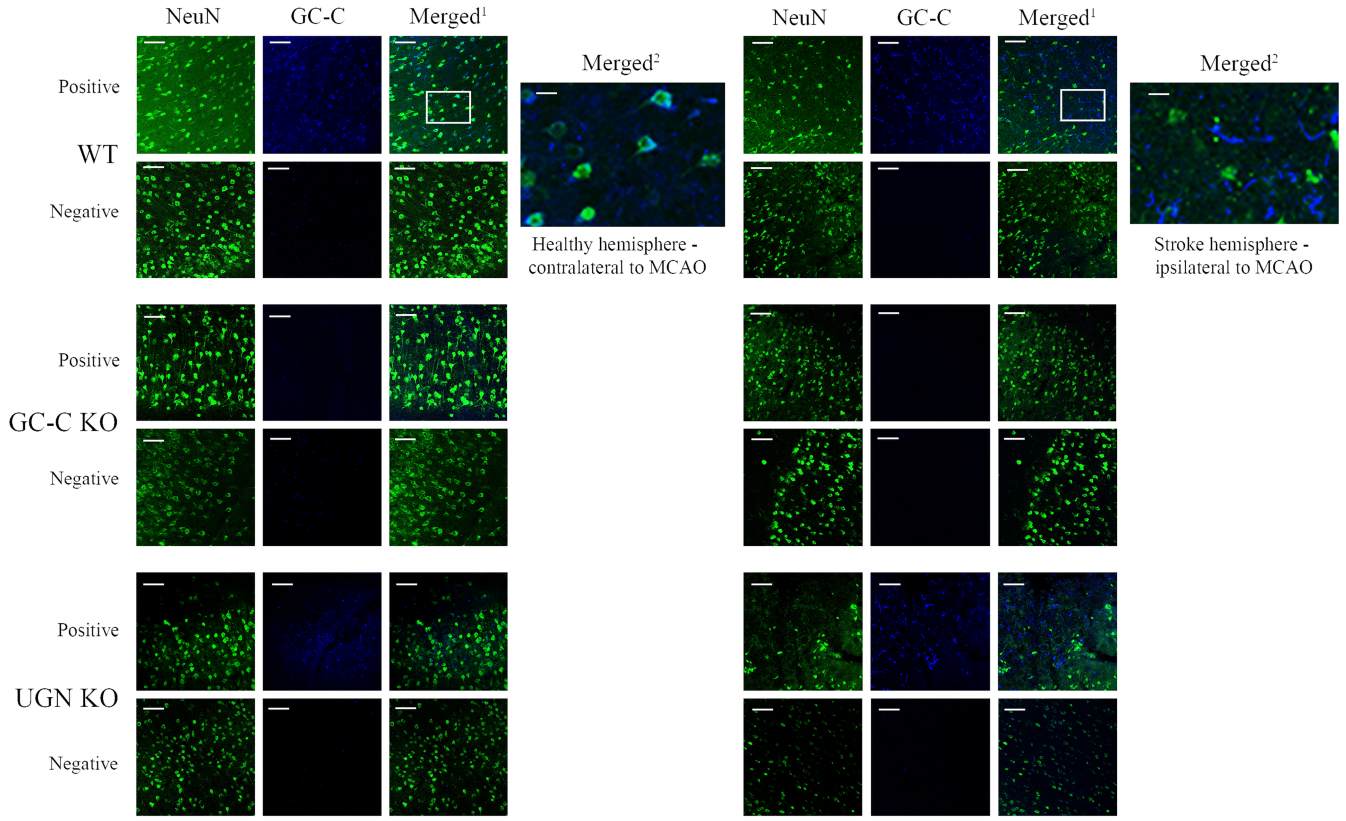

FIGURE 6 GC-C is expressed in cortical neurons of the contralateral, but not the ipsilateral hemisphere. The localisation of GC-C in the neurons was done by immunohistochemical staining of the ipsilateral peri-ischaemic region and corresponding contralateral cortical areas of WT, GC-C KO and UGN KO animals with GC-C and NeuN antibodies. In the contralateral hemisphere of both wild-type (WT) and UGN KO animals, GC-C expression was co-localised with NeuN, indicating that GC-C was expressed in cortical neurons in areas unaffected by stroke. In the peri-ischaemic area, GC-C no longer co-localised with NeuN in either animal strain and was expressed in another cell type. Brain slices from GC-C KO animals were used as a negative control. Positive: slices were stained with GC-C antibody. Negative: without GC-C antibody. Merged[1]: merged images of NeuN and GC-C staining. The bar represents 50 μm. Merged[2]: enlarged parts of Merged[1] images; the bar represents 1 0 μm

cells), whereas no co-localisation of GC-C mRNA with GFAP-positive cells was found in the cortex of the contralateral hemisphere.

4 | DISCUSSION

Previous research has established a neuroprotective effect of GC-A agonists in ischaemia and has shown no influence of GC-B agonists (Dobrivojević et al., 2012). Therefore, the primary goal of this study was to verify whether UGN, as a GC-C agonist, exerts an influence on stroke development. First, to determine the effects of UGN and GC-C on the ischaemic lesion and oedema size, MCAO was performed in four groups of mice (GC-C WT, GC-C KO, UGN WT, UGN KO). As expected, all animal groups showed a significant increase in ipsilateral hemisphere volume, compared with ipsilateral BL measurements (Dobrivojević et al., 2016; Okar et al., 2020). However, only GC-C KO animals showed a smaller lesion size compared with WT littermates. Based on these results, it seems that the activation of GC-C increases lesion size, contrary to the effect of GC-A agonists, which suggests a different function of individual natriuretic peptides in physiological as well pathophysiological conditions. Even though the size of the lesion differs in GC-C KO animals, there was no difference in neurological deficit severity between tested animals. There was a positive correlation between the severity of the symptoms and the size of the lesion in all tested animals 24 and 48 h after MCAO.

Because a possible reason for the shown differences in ischaemic lesion size could be the increased blood pressure showed in UGN KO animals compared with their WT littermates (Lorenz et al., 2003), we measured the blood pressure in all tested groups of animals. In the present study, we could not repeat the published results by Lorenz et al. The difference in systolic, diastolic and

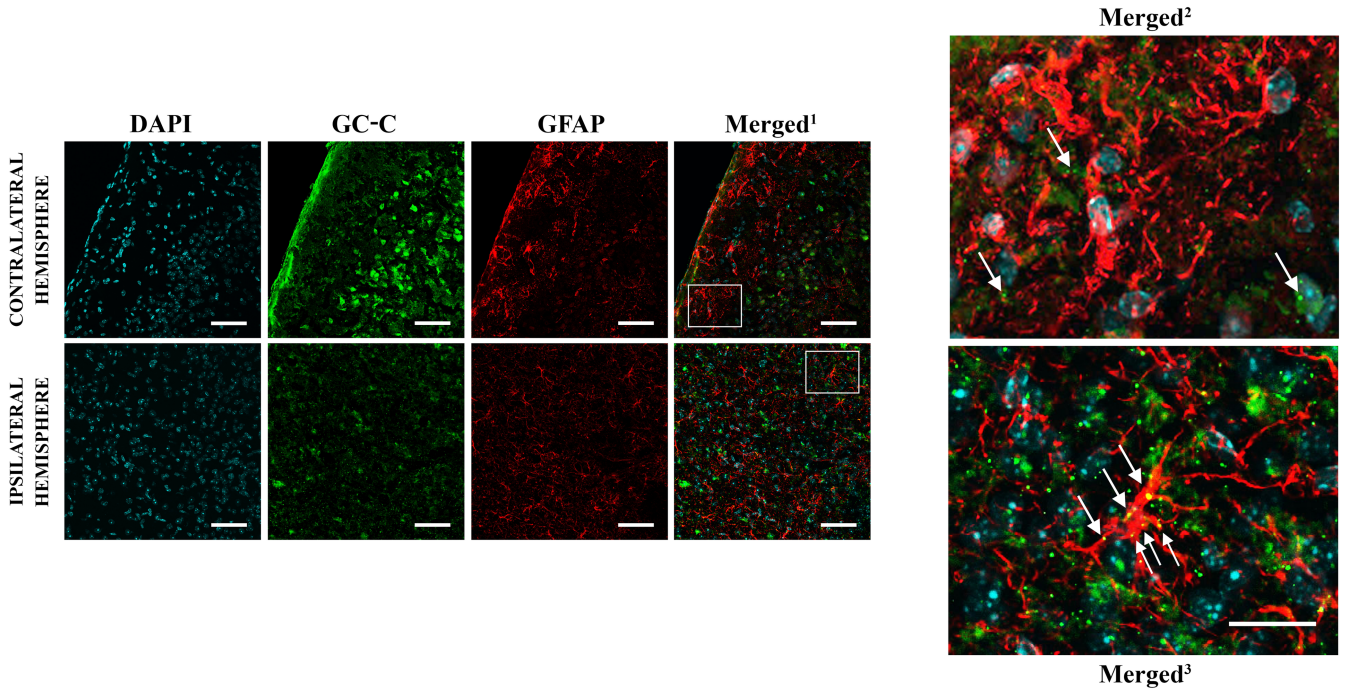

FIGURE 7 GC-C mRNA is localised in peri-ischaemic cortical astrocytes but not in the contralateral hemisphere of wild-type (WT) mice 48 h after MCAO. RNAScope® assay with a GC-C probe was performed along with immunohistochemical staining with a GFAP antibody in both ipsilateral and contralateral hemispheres. GC-C mRNA was expressed in peri-ischaemic astrocytes (Merged^3, white arrows), whereas GC-C was not present in astrocytes of the contralateral hemisphere (Merged^2, white arrows). Merged^1: merged images of GC-C, GFAP and DAPI staining; bar represents 50 μm. Merged^2 and Merged^3: the enlarged images of astrocytes in the contralateral cortex and a peri-ischaemic area, respectively, stained with DAPI, GC-C and GFAP; bar represents 20 μm. DAPI, 4′,6-diamidino-2-phenylindole; GC-C, guanylate cyclase C; GFAP, glial fibrillary acidic protein

MAP was observed in GC-C KO compared with WT littermates, but not in UGN KO animals. There was no difference in heart rate, tail blood volume or tail blood flow. The difference in blood pressure was not seen when separate strains of animals were compared, confirming the importance of using littermates when KO animals are studied. The possible reason for the observed discrepancies between published results and our study could be the difference in animal age. We used 30-week-old mice, whereas the animals used in the Lorenz study were much younger (15–23 weeks).

A special concern raised the recent publication of Thakkar et al. (2020) suggesting that the increased MAP leads to a decrease in lesion size in rats. For a 10 mmHg increase in MAP, the lesion size was smaller by 10%. In our study for the same difference in MAP, the difference in the size of the stroke lesion was more than 35%. In addition, there was no correlation between measured blood pressures and the size of the lesion or oedema. Furthermore, the MAP was higher in UGN KO animals, but they did not have the smallest lesion, suggesting, in addition to blood pressure, involvement of other factors in the development of the smaller lesions in GC-C KO animals. The difference in blood pressure among the tested animal groups did not affect the blood flow during MCAO, which is an important factor that could change the size of the lesion. The blood flow during MCAO was not correlated to the size of the stroke, suggesting the importance of the genetic strain of the animals and not the haemodynamics during MCAO or blood pressure differences.

Because the volumetric analysis of the ischaemic lesion pointed to a potentially harmful effect of GC-C activation during stroke, astrocytic Ca^{2+} response to UGN stimulation was examined to determine the role of both UGN signalling pathways, the GC-C-dependent or GC-C-independent, in the development of the ischaemic lesion. Our previous research showed that GC-C is predominantly expressed in neurons and is not expressed in astrocytes. UGN stimulation led to a similar Ca^{2+} response in cortical astrocytes of the contralateral hemispheres of both GC-C WT and GC-C KO animals, but no Ca^{2+} response upon UGN stimulation was observed in cortical neurons as shown previously (Habek et al., 2021). In physiological conditions, the Ca^{2+} signalling pathway of UGN in astrocytes is GC-C independent. The stronger Ca^{2+} response was obtained in cortical astrocytes of the peri-ischaemic region of the ipsilateral

hemisphere of WT animals when compared with their counterparts in the contralateral cortex.

The changes of Ca^{2+} signalling in the astrocytes during stroke development has been known for a while. It involves Ca^{2+}-dependent neurotransmitter release followed by neuronal excitability and toxicity in stroke (Ding, 2014). Furthermore, activation of the UGN Ca^{2+} dependent signalling pathway leads to extracellular acidification by activation of Na^+/H^+ exchanger (NHE) and bicarbonate transport in primary culture of mouse astrocytes (Habek et al., 2021). The involvement of NHE and bicarbonate transport in astrocytes in stroke development was previously shown (Kintner et al., 2004; Yao et al., 2016). Therefore, the increase in the Ca^{2+} signalling pathway in astrocytes in the peri-ischaemic area might be harmful by several different mechanisms for present and perturbed neurons in this area. The difference in Ca^{2+} signalling observed between peri-ischaemic astrocytes and astrocytes of the contralateral hemisphere in WT animals was not observed in GC-C KO mice, suggesting that lower Ca^{2+} response in those animals could lead to smaller ischaemic lesions.

The only possibility for GC-C to affect the Ca^{2+} response in cortical peri-infarct astrocytes is that those astrocytes should express GC-C after ischaemia, which we showed at protein and mRNA expression levels. The observed changes in Ca^{2+} response in the peri-ischaemic astrocytes 48 h after MCAO might be part of astrogliosis and glial scar formation (Barreto et al., 2011). Temporal regulation of GC-C expression has previously been shown in liver tissue as well, where GC-C expression became detectable only after liver injury or during the perinatal rapid liver growth (Mann et al., 2010; Scheving & Russell, 1996).

How can GC-C affect Ca^{2+} concentration in astrocytes? Activation of GC-C leads to an increase in intracellular cyclic guanosine monophosphate (cGMP) concentration. We predict that cGMP activates cyclic nucleotide-gated (CNG) channels, which might lead to the observed changes in Ca^{2+} signalling. CNGA2 channel expression has been confirmed in rodent astrocytes (Podda et al., 2012), and CNG expression is upregulated in astrocytes following ischaemic injury (Honsa et al., 2014).

It seems that the GC-C independent Ca^{2+} signalling pathway in astrocytes does not play a significant role in stroke development. The changes in Ca^{2+} response of UGN KO animals are quite different compared with GC-C KO animals or WT animals and those changes did not lead to differences in lesion size. Even though the Ca^{2+} response is similar, the rise in Ca^{2+} concentration is slower in both hemispheres but more prominent in the ipsilateral hemisphere, suggesting a generalised phenomenon. The changes in both ipsilateral and contralateral Ca^{2+} signalling in astrocytes were observed previously but no sooner than 7 days after photothrombosis (Takatsuru et al., 2013). The mechanism of this phenomenon is beyond the scope of this study.

5 | CONCLUSION

The UGN signalling pathways are changed during stroke and affect the size of the lesion and severity of stroke symptoms. GC-C is present in neurons in the cerebral cortex, whereas in the peri-ischaemic cortex, it is predominantly located in astrocytes where it affects Ca^{2+} signalling. GC-C KO mice have smaller ischaemic lesions, probably due to the decrease in Ca^{2+} signalling pathway activity, suggesting potentially harmful effects of this activation. The possible mechanisms could involve UGN activity on pH regulation in astrocytes through NHE activation and the subsequent worsening of existing interstitial post-ischaemic acidosis.

ACKNOWLEDGEMENTS

The research was funded by the Scientific Centre of Excellence for Basic, Clinical and Translational Neuroscience (project 'Experimental and clinical research of hypoxic–ischaemic damage in perinatal and adult brain'; GA KK01.1.1.01.0007 funded by the European Union through the European Regional Development Fund). The work of doctoral student Anja Barić has been fully supported by the 'Young researchers' career development project—training of doctoral students' and project BRADISCHEMIA (UIP-2017-05-8082) of the Croatian Science Foundation funded by the European Union from the European Social Fund.

CONFLICT OF INTEREST

The authors report no conflict of interest.

AUTHOR CONTRIBUTIONS

M. R. performed experiments, analysed data, wrote the manuscript and was involved in experimental design. N. H. assisted in performing live calcium imaging, immunohistochemical staining and RNAScope® assay. M. D. R. and H. J. performed MCAO experiments. S. Š. and A. B. conducted all MR imaging within the GlowLab Laboratory for Regenerative Medicine. A. D. designed experiments, analysed data, wrote and reviewed the manuscript.

PEER REVIEW

The peer review history for this article is available at https://publons.com/publon/10.1111/ejn.15674.

DATA AVAILABILITY STATEMENT

The raw data can be obtained upon request to the corresponding author.

ORCID

Nikola Habek https://orcid.org/0000-0002-7774-7386
Aleksandra Dugandžić https://orcid.org/0000-0001-9454-7207

REFERENCES

Anand-Srivastava, M. B. (2005). Natriuretic peptide receptor-C signaling and regulation. *Peptides*, *26*(6), 1044–1059. https://doi.org/10.1016/j.peptides.2004.09.023

Bamford, J., Sandercock, P., Dennis, M., Burn, J., & Warlow, C. (1991). Classification and natural history of clinically identifiable subtypes of cerebral infarction. *Lancet*, *337*(8756), 1521–1526. https://doi.org/10.1016/0140-6736(91)93206-O

Barone, F. C., & Feuerstein, G. Z. (1999). Inflammatory mediators and stroke: New opportunities for novel therapeutics. *Journal of Cerebral Blood Flow & Metabolism*, *19*, 819–834. https://doi.org/10.1097/00004647-199908000-00001

Barreto, G. E., Sun, X., Xu, L., & Giffard, R. G. (2011). Astrocyte proliferation following stroke in the mouse depends on distance from the infarct. *PLoS ONE*, *6*(11), e27881. https://doi.org/10.1371/journal.pone.0027881

Begg, D. P., Steinbrecher, K. A., Mul, J. D., Chambers, A. P., Kohli, R., Haller, A., Cohen, M. B., Woods, S. C., & Seeley, R. J. (2014). Effect of guanylate cyclase-C activity on energy and glucose homeostasis. *Diabetes*, *63*(11), 3798–3804. https://doi.org/10.2337/db14-0160

Belayev, L., Busto, R., Zhao, W., Fernandez, G., & Ginsberg, M. D. (1999). Middle cerebral artery occlusion in the mouse by intraluminal suture coated with poly-l-lysine: Neurological and histological validation. *Brain Research*, *833*(2), 181–190. https://doi.org/10.1016/S0006-8993(99)01528-0

Cao, L. H., & Yang, X. L. (2008). Natriuretic peptides and their receptors in the central nervous system. *Progress in Neurobiology*, *84*(3), 234–248. https://doi.org/10.1016/j.pneurobio.2007.12.003

Carrithers, S. L., Ott, C. E., Hill, M. J., Johnson, B. R., Cai, W., Chang, J. J., Shah, R. G., Sun, C., Mann, E. A., Fonteles, M. C., Forte, L. R., Jackson, B. A., Giannella, R. A., & Greenberg, R. N. (2004). Guanylin and uroguanylin induce natriuresis in mice lacking guanylyl cyclase-C receptor. *Kidney International*, *65*, 40–53. https://doi.org/10.1111/j.1523-1755.2004.00375.x

Chen, R., Xu, X., Huang, L., Zhong, W., & Cui, L. (2019). The regulatory role of long noncoding RNAs in different brain cell types involved in ischemic stroke. *Frontiers in Molecular Neuroscience*, *12*, 61. https://doi.org/10.3389/fnmol.2019.00061

Colantuoni, C., Lipska, B. K., Ye, T., Hyde, T. M., Tao, R., Leek, J. T., Colantuoni, E. A., Elkahloun, A. G., Herman, M. M., Weinberger, D. R., & Kleinman, J. E. (2011). Temporal dynamics and genetic control of transcription in the human prefrontal cortex. *Nature*, *478*(7370), 519–523. https://doi.org/10.1038/nature10524

Crane, M. R., Hugues, M., O'Hanley, P. D., & Waldman, S. A. (1992). Identification of two affinity states of low affinity receptors for *Escherichia coli* heat-stable enterotoxin: Correlation of occupation of lower affinity state with guanylate cyclase activation. *Molecular Pharmacology*, *41*, 1073–1080. PMID: 1352035.

Ding, S. (2014). Ca(2+) signaling in astrocytes and its role in ischemic stroke. *Advances in Neurobiology*, *11*, 189–211. https://doi.org/10.1007/978-3-319-08894-5_10

Dobrivojević, M., Sinđić, A., Edemir, B., Kalweit, S., Forssmann, W. G., & Hirsch, J. R. (2012). Interaction between bradykinin and natriuretic peptides via RGS protein activation in HEK-293 cells. *American Journal of Physiology-Cell Physiology*, *303*, 1260–1268. https://doi.org/10.1152/ajpcell.00033.2012

Dobrivojević, M., Špiranec, K., Gorup, D., Erjavec, I., Habek, N., Radmilović, M., Unfirer, S., Ćosić, A., Drenjančević, I., Gajović, S., & Sinđić, A. (2016). Urodilatin reverses the detrimental influence of bradykinin in acute ischemic stroke. *Experimental Neurology*, *284*, 1–10. https://doi.org/10.1016/j.expneurol.2016.07.007

Dugandžić, A., Ratko, M., & Habek, N. (2020). Anxiety-like behavior in female mice changes by feeding, possible effect of guanylate cyclase C. *European Journal of Neuroscience*, *52*, 2781–2790. https://doi.org/10.1111/ejn.14607

Estrada, V., Téllez, M. J., Moya, J., Fernández-Durango, R., Egido, J., & Fernández Cruz, A. F. (1994). High plasma levels of endothelin-1 and atrial natriuretic peptide in patients with acute ischemic stroke. *American Journal of Hypertension*, *7*, 1085–1089. https://doi.org/10.1093/ajh/7.12.1085

Folgueira, C., Beiroa, D., Callon, A., Al-Massadi, O., Barja-Fernandez, S., Senra, A., Fernø, J., López, M., Dieguez, C., Casanueva, F. F., Rohner-Jeanrenaud, F., Seoane, L. M., & Nogueiras, R. (2016). Uroguanylin action in the brain reduces weight gain in obese mice via different efferent autonomic pathways. *Diabetes*, *65*, 421–432. https://doi.org/10.2337/db15-0889

Fuller, F., Porter, J. G., Arfsten, A. E., Miller, J., Schilling, J. W., Scarborough, R. M., Lewicki, J. A., & Schenk, D. B. (1988). Atrial natriuretic peptide clearance receptor. Complete sequence and functional expression of cDNA clones. *The Journal of Biological Chemistry*, *263*, 9395–9401. https://doi.org/10.1016/S0021-9258(19)76554-5

Ganguly, U., Chaudhury, A. G., Basu, A., & Sen, P. C. (2001). STa-induced translocation of protein kinase C from cytosol to membrane in rat enterocytes. *FEMS Microbiology Letters*, *204*, 65–69. https://doi.org/10.1111/j.1574-6968.2001.tb10864.x

Garcia, J. H., Wagner, S., Liu, K. F., & Hu, X. J. (1995). Neurological deficit and extent of neuronal necrosis attributable to middle cerebral artery occlusion in rats. *Stroke*, *26*, 627–635. https://doi.org/10.1161/01.STR.26.4.627

Gąsecki, D., Kwarciany, M., Kowalczyk, K., Narkiewicz, K., & Karaszewski, B. (2020). Blood pressure management in acute ischemic stroke. *Current Hypertension Reports*, *23*, 3. https://doi.org/10.1007/s11906-020-01120-7

Gong, R., Ding, C., Hu, J., Lu, Y., Liu, F., Mann, E., Xu, C. M. B., & Luo, M. (2011). Role for the membrane receptor guanylyl cyclase-C in attention deficiency and hyperactive behavior. *Science*, *333*, 1642–1646. https://doi.org/10.1016/j.ygcen.2021.113797

González, R. G. (2006). Imaging-guided acute ischemic stroke therapy: From "time is brain" to "physiology is brain". *American Journal of Neuroradiology*, *27*, 728–735. PMID: https://www.ncbi.nlm.nih.gov/pubmed/16611754

Habek, N., Dobrivojević Radmilović, M., Kordić, M., Ilić, K., Grgić, S., Farkaš, V., Bagarić, R., Škokić, S., Švarc, A., & Dugandžić, A. (2020). Activation of brown adipose tissue in diet-induced thermogenesis is GC-C dependent. *Pflügers Archiv*, *472*(3), 405–417. https://doi.org/10.1007/s00424-020-02347-8

Habek, N., Ratko, M., & Dugandžić, A. (2021). Uroguanylin increases Ca^{2+} concentration in astrocytes via guanylate cyclase C-independent signaling pathway. *Croatian Medical Journal*, *62*, 250–263. https://doi.org/10.3325/cmj.2021.62.250

Honsa, P., Pivonkova, H., Harantova, L., Butenko, O., Kriska, J., Dzamba, D., Rusnakova, V., Valihrach, L., Kubista, M., & Anderova, M. (2014). Increased expression of hyperpolarization-activated cyclic nucleotide-gated (HCN) channels in reactive astrocytes following ischemia. *Glia*, *62*(12), 2004–2021. https://doi.org/10.1002/glia.22721

Hossmann, K. A., & Schuier, F. J. (1980). Experimental brain infarcts in cats. I. Pathophysiological observations. *Stroke*, *11*, 583–592. https://doi.org/10.1161/01.STR.11.6.583

Ikpa, P. T., Sleddens, H. F., Steinbrecher, K. A., Peppelenbosch, M. P., de Jonge, H. R., Smits, R., & Bijvelds, M. J. (2016). Guanylin and uroguanylin are produced by mouse intestinal epithelial cells of columnar and secretory lineage. *Histochemistry and Cell Biology*, *146*, 445–455. https://doi.org/10.1007/s00418-016-1453-4

Katan, M., Fluri, F., Schuetz, P., Morgenthaler, N. G., Zweifel, C., Bingisser, R., Kappos, L., Steck, A., Engelter, S. T., Muuler, B., & Christ-Crain, M. (2010). Midregional pro-atrial natriuretic peptide and outcome in patients with acute ischemic stroke. *Journal of the American College of Cardiology*, *56*(13), 1045–1053. https://doi.org/10.1016/j.jacc.2010.02.071

Kim, G. W., Lin, J. E., Snook, A. E., Aing, A. S., Merlino, D. J., Li, P., & Waldman, S. A. (2016). Calorie-induced ER stress suppresses uroguanylin satiety signaling in diet-induced obesity. *Nutrition & Diabetes*, *6*, e211. https://doi.org/10.1038/nutd.2016.18

Kintner, D. B., Su, G., Lenart, B., Ballard, A. J., Meyer, J. W., Ng, L. L., Shull, G. E., & Sun, D. (2004). Increased tolerance to oxygen and glucose deprivation in astrocytes from Na(+)/H(+) exchanger isoform 1 null mice. *American Journal of Physiology-Cell Physiology*, *287*, C12–C21. https://doi.org/10.1152/ajpcell.00560.2003

Kriz, J., & Lalancette-Hébert, M. (2009). Inflammation, plasticity and real-time imaging after cerebral ischemia. *Acta Neuropathologica*, *117*, 497–509. https://doi.org/10.1007/s00401-009-0496-1

Lai, T. W., Zhang, S., & Wang, Y. T. (2014). Excitotoxicity and stroke: Identifying novel targets for neuroprotection. *Progress in Neurobiology*, *115*, 157–188. https://doi.org/10.1016/j.pneurobio.2013.11.006

Leigh, R., Knutsson, L., Zhou, J., & van Zijl, P. C. (2018). Imaging the physiological evolution of the ischemic penumbra in acute ischemic stroke. *Journal of Cerebral Blood Flow & Metabolism*, *38*(9), 1500–1516. https://doi.org/10.1177/0271678X17700913

Li, P., Stetler, R. A., Leak, R. K., Shi, Y., Li, Y., Yu, W., Bennett, M. V. L., & Chen, J. (2018). Oxidative stress and DNA damage after cerebral ischemia: Potential therapeutic targets to repair the genome and improve stroke recovery. *Neuropharmacology*, *134*, 208–217. https://doi.org/10.1016/j.neuropharm.2017.11.011

Li, Y., Chopp, M., Chen, J., Wang, L., Gautam, S. C., Xu, Y. X., & Zhang, Z. (2000). Intrastriatal transplantation of bone marrow nonhematopoietic cells improves functional recovery after stroke in adult mice. *Journal of Cerebral Blood Flow & Metabolism*, *20*(9), 1311–1319. https://doi.org/10.1097/00004647-200009000-00006

López-Morales, M. A., Castelló-Ruiz, M., Burguete, M. C., Jover-Mengual, T., Aliena-Valero, A., Centeno, J. M., Alborch, E., Salom, J. B., Torregrosa, G., & Miranda, F. J. (2018). Molecular mechanisms underlying the neuroprotective role of atrial natriuretic peptide in experimental acute ischemic stroke. *Molecular and Cellular Endocrinology*, *472*, 1–9. https://doi.org/10.1016/j.mce.2018.05.014

Lorenz, J. N., Nieman, M., Sabo, J., Sanford, L. P., Hawkins, J. A., Elitsur, N., Gawenis, L. R., Clarke, L. L., & Cohen, M. B. (2003). Uroguanylin knockout mice have increased blood pressure and impaired natriuretic response to enteral NaCl load. *Journal of Clinical Investigation*, *112*(8), 1244–1254. https://doi.org/10.1172/JCI18743

Ma, Q., & Zhang, L. (2018). C-type natriuretic peptide functions as an innate neuroprotectant in neonatal hypoxic-ischemic brain injury in mouse via natriuretic peptide receptor 2. *Experimental Neurology*, *304*, 58–66. https://doi.org/10.1016/j.expneurol.2018.02.016

Makikallio, A. M., Makikallio, T. H., Korpelainen, J. T., Vuolteenaho, O., Tapanainen, J. M., Ylitalo, K., Sotaniemi, K. A., Huikuri, H. V., & Myllylä, V. V. (2005). Natriuretic peptides and mortality after stroke. *Stroke*, *6*, 1016–1020. https://doi.org/10.1161/01.STR.0000162751.54349.ae

Mann, E. A., Shanmukhappa, K., & Cohen, M. B. (2010). Lack of guanylate cyclase C results in increased mortality in mice following liver injury. *BMC Gastroenterology*, *10*, 86. https://doi.org/10.1186/1471-230X-10-86

Merlino, D. J., Barton, J. R., Charsar, B. A., Byrne, M. D., Rappaport, J. A., Smeyne, R. J., Lepore, A. C., Snook, A. E., & Waldman, S. A. (2019). Two distinct GUCY2C circuits with PMV (hypothalamic) and SN/VTA (midbrain) origin. *Brain Structure & Function*, *224*(8), 2983–2999. https://doi.org/10.1007/s00429-019-01949-y

Naruse, S., Aoki, Y., Takei, R., Horikawa, Y., & Ueda, S. (1991). Effects of atrial natriuretic peptide on ischemic brain edema in rats evaluated by proton magnetic resonance method. *Stroke*, *22*, 61–65. https://doi.org/10.1161/01.STR.22.1.61

Okar, S. V., Topcuoglu, M. A., Yemisci, M., Cakir Aktas, C., Oguz, K. K., & Arsava, E. M. (2020). Post-stroke inflammatory response is linked to volume loss in the contralateral hemisphere. *Journal of Neuroimmunology*, *344*, 577247. https://doi.org/10.1016/j.jneuroim.2020.577247

Pfeifer, A., Klatt, P., Massberg, S., Ny, L., Sausbier, M., Hirneiss, C., Wang, G. X., Korth, M., Aszódi, A., Andersson, K. E., Krombach, F., Mayerhofer, A., Ruth, P., Fässler, R., & Hofmann, F. (1998). Defective smooth muscle regulation in

cGMP kinase I-deficient mice. *The EMBO Journal*, *17*, 3045–3051. https://doi.org/10.1093/emboj/17.11.3045

Podda, M. V., Leone, L., Piacentini, R., Cocco, S., Mezzogori, D., D'Ascenzo, M., & Grassi, C. (2012). Expression of olfactory-type cyclic nucleotide-gated channels in rat cortical astrocytes. *Glia*, *60*(9), 1391–1405. https://doi.org/10.1002/glia.22360

Potter, L. R., Abbey-Hosch, S., & Dickey, D. M. (2006). Natriuretic peptides, their receptors, and cyclic guanosine monophosphate-dependent signaling functions. *Endocrine Reviews*, *27*, 47–72. https://doi.org/10.1210/er.2005-0014

Rubattu, S., Ridker, P. M., Stampfer, M., Hennekens, C. H., Volpe, M., & Lindpaintner, K. (1999). The gene encoding atrial natriuretic peptide and the risk of human stroke. *Circulation*, *100*, 1722–1726. https://doi.org/10.1161/01.CIR.100.16.1722

Rubattu, S., Stanzione, R., Di Angelantonio, E., Zanda, B., Evangelista, A., Tarasi, D., Gigante, B., Pirisi, A., Brunetti, E., & Volpe, M. (2004). Atrial natriuretic peptide gene polymorphisms and risk of ischemic stroke in humans. *Stroke*, *35*(4), 814–818. https://doi.org/10.1161/01.STR.0000119381.52589.AB

Scheving, L. A., & Russell, W. E. (1996). Guanylyl cyclase C is up-regulated by nonparenchymal cells and hepatocytes in regenerating rat liver. *Cancer Research*, *56*, 5186–5191. PMID: https://www.ncbi.nlm.nih.gov/pubmed/8912855

Sinđić, A., Dobrivojević, M., & Hirsch, J. R. (2011). Natriuretic peptides in brain physiology. *Translational Neuroscience*, *2*(3), 246. https://doi.org/10.2478/s13380-011-0029-y

Sindić, A., Velic, A., Başoglu, C., Hirsch, J. R., Edemir, B., Kuhn, M., & Schlatter, E. (2005). Uroguanylin and guanylin regulate transport of mouse cortical collecting duct independent of guanylate cyclase C. *Kidney International*, *68*(3), 1008–1017. https://doi.org/10.1111/j.1523-1755.2005.00518.x

Sobey, C. G. (2003). Bradykinin B2 receptor antagonism: A new direction for acute stroke therapy? *British Journal of Pharmacology*, *139*, 1369–1371. https://doi.org/10.1038/sj.bjp.0705415

Takatsuru, Y., Eto, K., Kaneko, R., Masuda, H., Shimokawa, N., Koibuchi, N., & Nabekura, J. (2013). Critical role of the astrocyte for functional remodeling in contralateral hemisphere of somatosensory cortex after stroke. *The Journal of Neuroscience: The Official Journal of the Society for Neuroscience*, *33*(11), 4683–4692. https://doi.org/10.1523/JNEUROSCI.2657-12.2013

Thakkar, P. C., McGregor, A. L., Barber, P. A., Paton, J., Barrett, C. J., & McBryde, F. D. (2020). Therapeutic relevance of elevated blood pressure after ischemic stroke in the hypertensive rats. *Hypertension*, *75*(3), 740–747. https://doi.org/10.1161/HYPERTENSIONAHA.119.14219

Valentino, M. A., Lin, J. E., Snook, A. E., Li, P., Kim, G. W., Marszalowicz, G., Magee, M. S., Hyslop, T., Schulz, S., & Waldman, S. A. (2011). A uroguanylin-GUCY2C endocrine axis regulates feeding in mice. *Journal of Clinical Investigation*, *121*(9), 3578–3588. https://doi.org/10.1172/JCI57925

Wang, F., Flanagan, J., Su, N., Wang, L. C., Bui, S., Nielson, A., Wu, X., Vo, H. T., Ma, X. J., & Luo, Y. (2012). RNAscope: A novel in situ RNA analysis platform for formalin-fixed, paraffin-embedded tissues. *The Journal of Molecular Diagnostics*, *14*, 22–29. https://doi.org/10.1016/j.jmoldx.2011.08.002

Yao, H., Azad, P., Zhao, H. W., Wang, J., Poulsen, O., Freitas, B. C., Muotri, A. R., & Haddad, G. G. (2016). The $Na^+/HCO3^-$ co-transporter is protective during ischemia in astrocytes. *Neuroscience*, *339*, 329–337. https://doi.org/10.1016/j.neuroscience.2016.09.050

Zhao, X., Ho, D., Gao, S., Hong, C., Vatner, D. E., & Vatner, S. F. (2011). Arterial pressure monitoring in mice. *Current Protocols in Mouse Biology*, *1*, 105–122. https://doi.org/10.1002/9780470942390.mo100149

How to cite this article: Ratko, M., Habek, N., Dobrivojević Radmilović, M., Škokić, S., Justić, H., Barić, A., & Dugandžić, A. (2022). Role of uroguanylin's signalling pathway in the development of ischaemic stroke. *European Journal of Neuroscience*, *56*(1), 3720–3737. https://doi.org/10.1111/ejn.15674